Large-scale exploration of whole-brain structural connectivity in anorexia nervosa: alterations in the connectivity of frontal and subcortical networks

Authors: E. Caitlin Lloyd, PhD[1,2*]; Karin E. Foerde, PhD[1,2]; Alexandra F. Muratore, PhD[1,2]; Natalie Aw, MS[1,2]; David Semanek, BA[1,2]; Joanna E. Steinglass, MD[1,2]; Jonathan Posner, MD[3]

Affiliations:

[1]Department of Psychiatry, Columbia University Irving Medical Center, New York, NY, USA

[2]New York State Psychiatric Institute, New York, New York, NY, USA

[3]Department of Psychiatry, Duke University, Durham, NC, USA

*Corresponding author: Dr Caitlin Lloyd

Address: Department of Psychiatry, Columbia University Irving Medical Center, New York, NY, USA.

Phone: 646-774-8201

Email: caitlin.lloyd@nyspi.columbia.edu

Abstract:

Anorexia nervosa (AN) is characterised by disturbances in cognition and behaviour surrounding eating and weight, which may relate to the structural connectivity of the brain that supports effective information processing and transfer. In the current investigation, diffusion-weighted MRI data acquired from female patients with AN (n = 148) and female healthy controls (HC; n = 119), aged 12-40 years, were combined across five cross-sectional studies. Probabilistic tractography was completed, and full cortex connectomes describing streamline counts between 84 brain regions generated and harmonised. The network-based statistic tested between-group differences in connectivity strength of brain subnetworks. Whole-brain connectivity of brain regions was indexed using graph theory tools, and compared between groups using multiple linear regression. Associations between structural connectivity variables that differed between groups, and illness severity markers, were explored amongst AN patients using multiple linear regression. Statistical models included age, motion, and study as covariates. The network-based statistic indicated AN patients, relative to HC, had reduced connectivity in a network comprising subcortical regions and greater connectivity between frontal cortical regions ($p < 0.05$, FWE corrected). Graph theory analyses supported reduced connectivity of subcortical regions, and greater connectivity of left occipital cortex, in patients relative to HC ($p < 0.05$, permutation corrected). Reduced subcortical network connectivity was associated with lower BMI among the AN group. Collectively, the findings suggest that structural differences in subcortical and cortical networks are present in AN, and may reflect illness mechanisms.

Background

Anorexia nervosa (AN) is characterised by abnormal behaviour and cognition surrounding eating and weight, including persistent restriction of food intake, fear of gaining weight or of becoming fat, and distorted self-image(1). The illness has high rates of mortality (2), physical and psychiatric morbidity (3, 4), and severe effects on quality of life (5). The efficacy of current treatments for AN is limited, and relapse rates are high (6). Improvement in outcome is likely to depend on an improved understanding of the neural underpinnings of illness, including understanding the structural architecture of the brain in AN. To address existing gaps in knowledge, this study examined the structural (white matter) connectivity across the whole brain in AN. Diffusion-weighted MRI (dMRI) data from five studies were pooled to compare a large sample of individuals with AN and healthy control participants (HC).

The brain operates as a large-scale system comprising densely connected and interacting brain regions. Co-ordinated patterns of activation, or functional connectivity, across spatially diffuse brain regions facilitates the information processing and integration that is necessary for behaviour and cognition across a range of domains, including visual memory and attention (7), language (8), and cognitive/inhibitory control (9). Structural, or white matter, connections support functional connectivity across the brain (10, 11). Analysis of structural connectivity can be a fruitful approach to identifying functionally significant biological correlates of illness in AN.

White matter connectivity may be studied in vivo using dMRI (12). To date, most dMRI studies of AN have focused on the microstructural properties of white matter (13), which describe the

quality of nerve cell axons but do not provide information about connectivity between regions of the brain. Studies that have compared connections between brain regions in individuals with AN relative to HC have typically focused on a small number of white matter tracts or connections (13, 14). This approach could mean that important between-group differences are missed because they were not included in a priori hypotheses. As the neuropathological basis of AN is relatively unclear, additional data-driven approaches are warranted.

Whole-brain approaches explore structural connectivity across the entire brain. Pairwise structural connections between all regions of the brain can be represented in the structural connectome, a construct derived via mathematical graph theory. The structural connectome (15) contains "nodes" (brain regions) and "edges" (the white matter connections between brain regions). Using mathematical graph theory tools, regional, subnetwork, and whole-brain, connectivity properties can be quantified, to describe characteristics of the brain system that affect information transfer. There are few structural connectome studies of AN. Those that do exist are generally small (16), though the single large study (including 96 AN and 96 HC; (17)) reported increased white matter integrity within parietal and occipital subnetworks. Existing structural connectome investigations in AN populations have typically used a tract reconstruction method that estimates a single fibre orientation within each voxel. This approach can lead to misrepresentation of the white matter tracts, since white matter often contains complex fibre architectures such as bending or crossing fibres (18, 19). More accurate reconstructions are obtained by modelling multiple fibres per voxel, as probabilistic tractography algorithms do (20). Probabilistic methods have the additional advantage of accounting for the noise inherent in dMRI data, and consequent uncertainty in the tract reconstruction process.

The aim of the current study was to leverage advances in dMRI methods, including the application of a probabilistic algorithm for tract reconstruction, to explore brain-wide structural connectivity in a large sample of patients with AN and HC. In addition to considering the strength of white matter connections between brain regions, we probed differences in how connected brain regions are with the rest of the brain (i.e., node connectivity). This approach offers a window into brain organisation differences that may contribute to psychopathology in AN.

Participants and Methods

Analysis of dMRI data collected from 267 participants in five different cross-sectional studies (14, 21-24) was undertaken. Data from a subsample of participants from one of these studies (22 AN, 18 HC) were included in a prior publication comparing specific frontostriatal tracts between AN and HC (14); other dMRI data (for 122 AN, 101 HC) are unpublished.

Participants

Participants were 148 females who met DSM-5 criteria for AN, and 119 female HC. All participants were between the ages of 12 and 40 years. Exclusion criteria across all studies were: presence of psychotic disorder, current substance use disorder, history of a neurological disorder/injury, estimated IQ less than 80, and MRI contraindications. Additional exclusion criteria for HC included current/past psychiatric illness, significant medical conditions, and body mass index (BMI) outside of the 18.5-25 kg/m^2 range. Aside from 11 participants, all were free from psychotropic medication use at the time of MRI scanning. Medication included selective

serotonin reuptake inhibitors (n = 1), serotonin and noradrenaline reuptake inhibitors (n = 1), and tricyclic antidepressants (n = 1). Eating disorder diagnoses were made by the Eating Disorder Examination (25) or Eating Disorder Diagnostic Assessment for DSM-5 (26). Co-occurring diagnoses were assessed (for adults) by Structured Clinical Interview for DSM-IV or 5 (27, 28), and (for adolescents) by the Schedule for Affective Disorders and Schizophrenia for School-Aged Children (29). Height and weight were measured on the day of the MRI scan for calculation of BMI. Each study was approved by the New York State Psychiatric Institute (NYSPI) Institutional Review Board. Researchers provided a complete description of the study to participants, following which adult participants provided written informed consent, and adolescents provided written assent with parental consent.

Amongst the AN patients, 85 (57.4%) were diagnosed with the restricting subtype. All adult AN participants, and a subset of adolescent AN participants, received inpatient or outpatient treatment at NYSPI. HC were recruited from the community.

MRI procedures

Scanning parameters

The MRI scanner and DWI scanning parameters were study-specific and are described in the Supplement (Table S1).

MRI Image processing

Anatomical images

Structural images were processed using the automated Freesurfer pipeline (30, 31), which includes motion correction, brain extraction, Talairach transformation and intensity

normalisation. Grey matter regions were parsed into 84 distinct regions based on the Desikan-Killany atlas (32).

The parcellated image was used to generate a five-tissue type image, in which white matter, cortical and subcortical grey matter, cerebral spinal fluid (CSF), and pathological tissue are distinguished. Anatomical images were warped into diffusion space using a rigid body transformation performed with FSL's flirt method (50, 51), followed by a non-linear normalization using ANTS (52, 53), and resampled such that the voxel size was 1.25 mm^3.

Diffusion images

Each scan was visually checked for artifacts prior to image pre-processing, and volumes containing artifacts were removed. When more than 25% of the total volumes were removed, the participant was excluded (n = 3 AN, 0 HC). A fully automated image pre-processing pipeline implemented in MRtrix3 (33) was applied to the data, including: denoising, gibbs-artifact removal, B0 susceptibility-induced distortion correction, eddy current and motion correction (using the FSL eddy tool; (34)), and B1 field inhomogeneity correction (using the ANTS N4 algorithm; (35)). When a pair of B0 images with opposite phase encoding was available, the inhomogeneity field was estimated and applied to the DWI data using the eddy topup and apply topup tools (36) during the eddy current/motion correction phase. Where fieldmap images were available but B0 image pairs were not, distortion correction was applied prior to the processing pipeline by applying a representative affine transformation to all DWI volumes using FSL's epi_reg command (37, 38). The preprocessed dMRI data were up-sampled to an isotropic voxel size of 1.25 mm^3. Motion was quantified with average framewise displacement across the dMRI scan and did not differ between AN and HC participants: HC=0.16 (SD=0.1), AN = 0.18

(SD=0.15); $t(265) = 1.09$, $p = 0.276$. Details of average framewise displacement by diagnostic group and study are available in the Supplement (Table S2).

Probabilistic Tractography

Anatomically-constrained probabilistic tractography was completed through application of a standard MRtrix3 pipeline (33). First, response functions of white matter, grey matter and CSF were derived with the dhollander algorithm (39), using the dMRI signal and the five-tissue type image generated from the structural MRI scan. Next, the response functions of white matter fibres were estimated in the voxels with the 300 greatest fractional anisotropy values (indicative of more directed diffusion). Using the dMRI signal and the calculated response functions, the underlying distribution of fibres in each voxel was recovered using multi-shell multi-tissue constrained spherical deconvolution (40), with default maximum spherical harmonic degree parameters. This approach allows dMRI signal resulting from white matter and CSF components to be distinguished, preventing CSF contaminating estimates of white matter fibre orientation distributions. Consequently, the influence of partial volume effects (e.g., due to brain atrophy in AN) on tract reconstruction was minimised. White matter fibre orientation distributions were normalised, to remove residual inhomogeneity in intensities. Seed points for streamlines were determined dynamically. Seeding continued until 20,000,000 streamlines between 10 and 250 mm were generated. Streamline step size was 0.625 mm; the maximum angle between successive steps was 22.5 degrees.

The iFOD2 tracking algorithm (41) determines the probability of candidate streamline paths by sampling fibre orientation distributions along the entire path. More probable, and thus reconstructed, streamlines are generally those where fibre orientation distribution amplitudes along the path are large. The tractography was anatomically constrained, with the five-tissue type

image used as a biological prior to guide streamline termination and acceptance (42). Streamlines were re-tracked if a poor termination was encountered, and cropped at the grey matter white matter interface.

Graph construction

Graphs can provide a mathematical representation of the brain network, or structural connectome. To create brain graphs, a network node was assigned to each of the 84 regions from the anatomical parcellation. For each participant, the number of streamlines between all possible pairs of regions (Ni, Nj) was counted to provide edge values, generating an undirected, weighted, graph that quantified connectivity strength within each tract of the brain. Streamline endpoints were mapped to nodes within a 4mm radius of the endpoint. When no streamlines connected a pair or regions, the edge value was set to 0.

Individual graphs (or connectomes) were harmonised using the R implementation of neuroCombat (43, 44), to remove effects of differences in scanner/scan parameters across and within studies. To retain effects of diagnosis, age and BMI, these variables were specified as covariates in the harmonisation model. In exploratory analyses probing subtype differences in structural connectivity, the harmonisation model was applied to data from AN patients only, and included subtype as an additional covariate. Following recent recommendations graphs were not thresholded prior to completing network and graph theory analyses (45).

Data analysis

Streamline counts between brain regions comprised the measure of connectivity in the current study.

Network-based statistic (46)

Edge-wise connectivity was compared between AN and HC groups using the network-based statistic method implemented in Matlab (https://sites.google.com/site/bctnet/comparison/nbs; (47)). To complete the network-based statistic analysis, a t-test was performed to test group differences at each connection, or edge, to create an 84 x 84 matrix of t-scores. The t-score matrix was thresholded to identify connections with a between-group difference t-score greater than 3.1, which corresponds to a p value of 0.001. This relatively stringent threshold reduces the risk of detecting false positive effects. Sets of supra-threshold edges that are connected (components) are identified. Permutation testing derives p-values for a test of the hypothesis that the size of components differing in connectivity strength between groups is larger than what would be expected if there was no between group difference: for each permutation, the group to which each participant belongs is randomly exchanged, the test statistic computed for group differences at each edge, and the size of the maximal supra-threshold component stored. The null distribution of the maximum component size can be then empirically estimated and used to compute a p-value for the observed components (i.e., those identified in the unpermuted data). 10,000 permutations were specified, and identified components were significant at a family-wise error corrected rate of $p < 0.05$. The network-based statistical analysis was completed for the contrasts HC > AN, and AN > HC; p-values were Bonferroni corrected for two tests. Models were adjusted for age, motion and study. Study was included as a covariate given the potential for residual batch effects to remain following harmonisation.

Node-based analyses

Two measures of regional network topology, nodal *strength* and *efficiency*, were computed for each network node (or brain region), using the BCT toolbox (https://sites.google.com/site/bctnet/) in Matlab (47, 48). Strength is the total number of connections (streamlines) of each node, and was calculated as the sum of the node's streamline connections. Efficiency describes the ease at which information can move from one region to another within a network of the node's neighbours ("ease" here refers to fewer intermediary nodes). To calculate efficiency, the average inverse of the shortest path length between all nodes directly connected to the node in question was determined. Path length was defined as the inverse of streamline count. The contribution of a given path to the efficiency calculations was proportionate to the streamline count between the path nodes and the node for which efficiency was calculated (i.e. the average was weighted). *Global efficiency*, the ease at which information can move from one region to any other region on average across the whole brain, was also calculated.

Node characteristics were compared between AN and HC in linear regression models adjusted for age, motion and study. Permutation tests established statistical significance and corrected for multiple comparisons across the 84 nodes (with the minP method), using the R package Permuco (49). 10,000 permutations for each test were specified; the Freedman-Lane procedure managed effects of nuisance variables (age, motion and study). A linear regression model adjusted for age, motion and study compared AN and HC groups on the global efficiency metric.

The tractography, connectome generation, connectome metric calculation and analysis procedures are detailed in Figure 1.

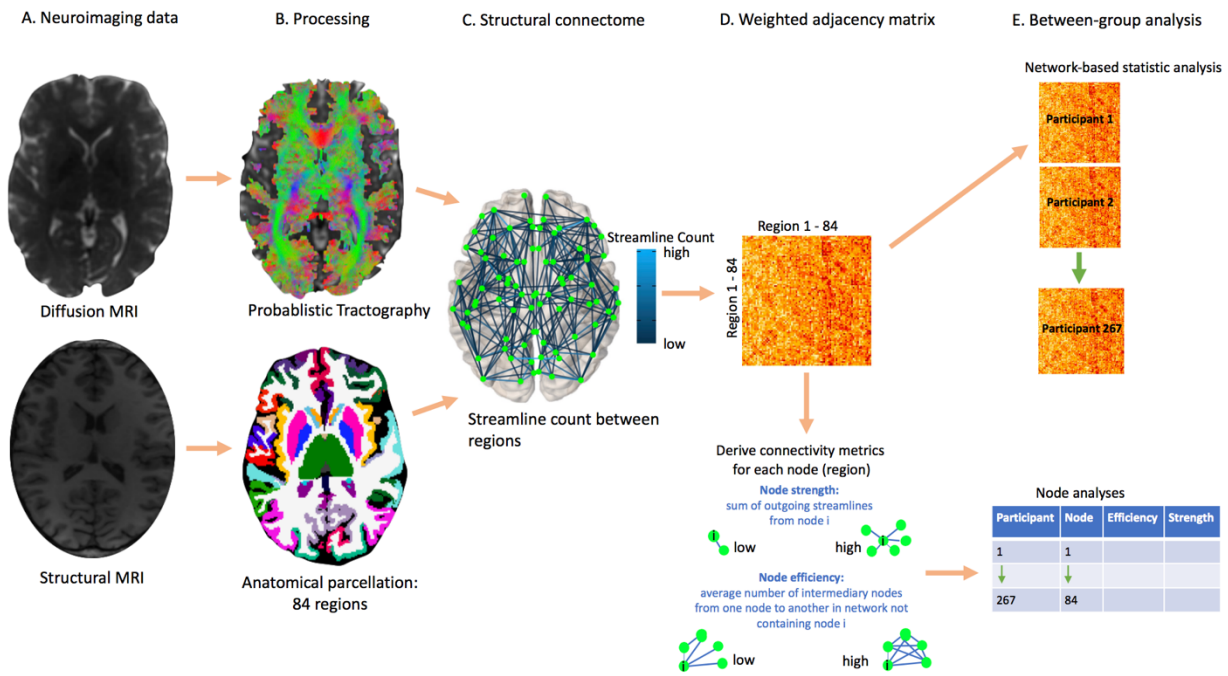

Figure 1: Neuroimaging and analysis methods of the current study
For each participant, a diffusion MRI and structural MRI scan were acquired (panel A). White matter tracts in the brain were reconstructed using a probabilistic tracking algorithm applied to diffusion MRI data, and the structural brain image was parcellated into 84 regions (panel B). Combining the tractography output with the brain parcellation allowed the creation of a structural connectome for each participant, which described the number of streamlines between each pair of regions (panel C). This information was represented in a weighted adjacency matrix, which was used to calculate node metrics (panel D). Anorexia nervosa and healthy control groups were compared on the strength of structural connections and node metrics, across the whole brain (panel E).

The main analyses probing group differences in graph theory metrics and subnetwork connectivity were repeated using the unharmonised data. This was to verify whether findings were consistent when different methods were used to combine data across the five studies, which would support the robustness of study conclusions.

Exploratory analyses

Association of structural connectome metrics and AN severity

Network components and node metrics that significantly differed between groups ($p < 0.05$, corrected) were tested for associations with BMI and illness duration within the AN group only. For each component reaching statistical significance, the mean number of streamlines across edges of these components was calculated. To combine BMI for adults and BMI percentile for adolescents, scaled scores (mean centred) were created in each group, using BMI for individuals over 19, and BMI percentiles for individuals 19 and under. Component connectivity metrics were regressed onto BMI and illness duration, in separate models, in the patient sample. Using the same method, node metrics that differed between groups were tested for their association with clinical variables amongst individuals with AN. All statistical models were adjusted for motion, age and study. Models involving the regression of illness duration were additionally adjusted for the scaled BMI variable. Model predictors and outcomes (aside from the already scaled BMI variable) were mean centred and scaled, for comparison of effect estimates across exploratory analyses.

Subtype differences in structural connectome metrics

Subtype differences in component connectivity and node metrics were explored by regressing outcomes that differed between AN and HC groups onto subtype, in linear regression models adjusted for motion, age, study, and the scaled BMI variable.

Code and data availability

The code for dMRI data preprocessing, tractography, and analysis, steps is available on github: https://github.com/CaitlinLloyd/Anorexia.Nervosa_Tractography. Data for between group differences in streamline counts between all pairs of regions are available as Supplementary material (see Supplementary Tables file), for harmonised and unharmonised data.

Results

Participant characteristics

Participant characteristics are displayed in Table 1. For a summary of results by study and diagnosis, see the Supplement (Table S2).

Table 1: Demographic and clinical characteristics of study participants

Variable	**HC (n = 119)**	**AN (n = 148)**
Age (years)	21·03 (5·11)	20·34 (6·21)
BMI (kg/m^2)[a]	21·49 (1·69)	16·08 (1·97)
BMI percentile (%)[b]	47·74 (23·38)	9·6 (10·5)
STAI (T)	30·11 (6·96)	59·7 (11·35)
BAI	3·39 (4·51)	21·35 (12·25)
BDI	1·42 (2·01)	26·19 (12·16)
EDEQ Eating Concerns[a]	0·1 (0·28)	3·13 (1·62)
EDEQ Restraint[a]	0·27 (0·6)	3·9 (1·91)
EDEQ Shape Concerns[a]	0·37 (0·5)	4·39 (1·61)
EDEQ Weight Concerns[a]	0·33 (0·5)	4·18 (1·68)
EDEQ Global score	0·27 (0·39)	3·9 (1·54)
Illness Duration (years)	NA	59·1 (69.65)

[a] BMI information presented for participants **over 19** (n for AN: 70, n for HC: 77) [b] BMI percentile information presented for participants **19 and under** (n for AN: 78, n for HC: 42)
BAI: Beck anxiety inventory, BDI: Beck depression inventory, BMI: Body mass index; EDEQ: Eating disorder examination questionnaire, STAI T: Spielberger state-trait anxiety inventory trait anxiety subscale

Network-based statistic

The network-based statistic indicated one component with stronger connectivity amongst HC compared to AN. This component included 11 connections between subcortical regions (p = 0.026). Conversely, the network-based statistic indicated one component that was stronger amongst individuals with AN relative to HC. This component included 8 connections between regions generally located in the frontal cortex (p = 0.042). The network-based statistic analysis results are displayed in Figure 2. Details of average connectivity within the subcortical and cortical components, by study and diagnosis, are presented in the Supplement (Table S3, Figures S1 and S2).

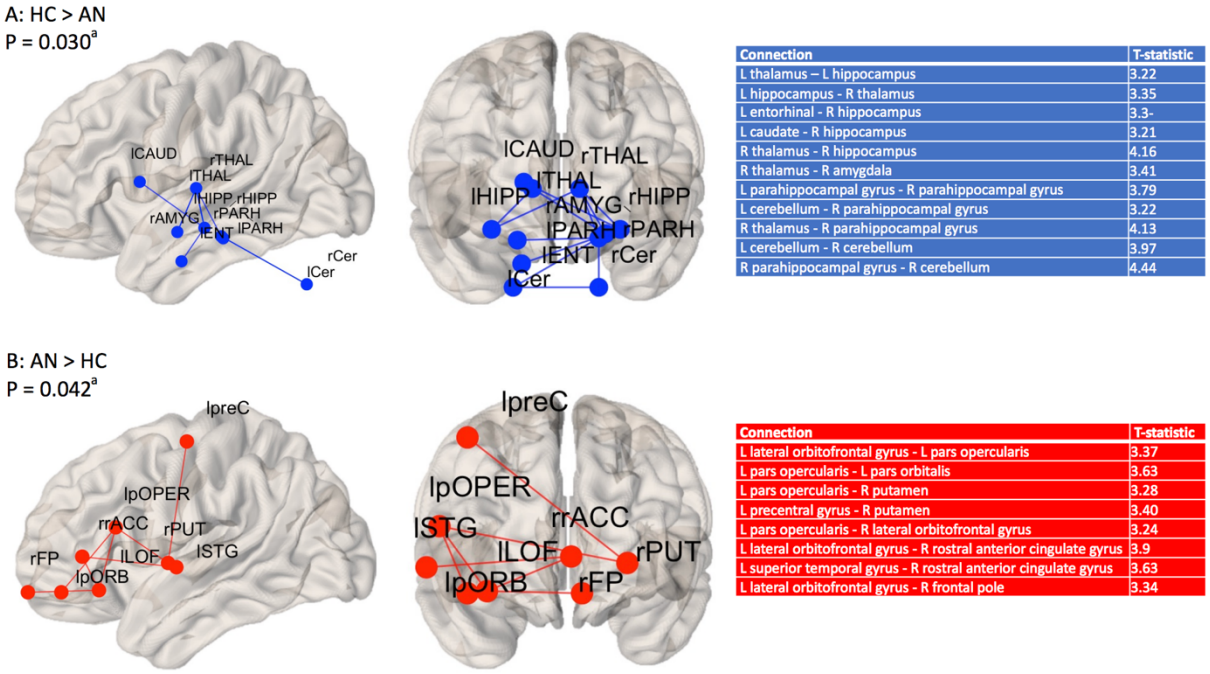

Connection	T-statistic
L thalamus – L hippocampus	3.22
L hippocampus - R thalamus	3.35
L entorhinal - R hippocampus	3.3-
L caudate - R hippocampus	3.21
R thalamus - R hippocampus	4.16
R thalamus - R amygdala	3.41
L parahippocampal gyrus - R parahippocampal gyrus	3.79
L cerebellum - R parahippocampal gyrus	3.22
R thalamus - R parahippocampal gyrus	4.13
L cerebellum - R cerebellum	3.97
R parahippocampal gyrus - R cerebellum	4.44

Connection	T-statistic
L lateral orbitofrontal gyrus - L pars opercularis	3.37
L pars opercularis - L pars orbitalis	3.63
L pars opercularis - R putamen	3.28
L precentral gyrus - R putamen	3.40
L pars opercularis - R lateral orbitofrontal gyrus	3.24
L lateral orbitofrontal gyrus - R rostral anterior cingulate gyrus	3.9
L superior temporal gyrus - R rostral anterior cingulate gyrus	3.63
L lateral orbitofrontal gyrus - R frontal pole	3.34

Figure 2: Results of the network-based statistic analysis
Panel A shows the component comprising tracts that had higher streamline counts in healthy control participants compared to AN patients. Panel B shows the component comprising tracts that had higher streamline counts in AN patients compared to healthy control participants. AN: anorexia nervosa, HC: healthy controls, lLOF: left lateral orbitofrontal gyrus, lpOPER: left pars opercularis, lpORB: left pars orbitalis, lpreC: left precentral gyrus, lSTG: left superior temporal gyrus' rFP: right frontal pole, rPUT: right putamen, rrACC: right rostral anterior cingulate gyrus, lCer: left Cerebellum, lFP: left frontal pole, lLOF: left lateral orbitofrontal gyrus, lPARH: left parahippocampal gyrus, lTHAL: left thalamus, rHIPP: right hippocampus, rPARH: right parahippocampal gyrus, rTHAL: right thalamus.

Node-based analyses

Node-based analyses indicated that individuals with AN, relative to HC, had reduced strength of the left hippocampus (B = -2367.69, [95% CI: -3549.32, -1186.06], p = 0.008), left cerebellum (B = -2420.77, 95% CI: [-3646.02, -1195.52], p = 0.024), left parahippocampal gyrus (B = -1284.7, 95% CI: [-1992.31, -577.08], p = 0.024), right cerebellum (B = -2361.14, 95% CI: [-3618.19,-1104.09], p = 0.024), and greater strength of the left lateral occipital gyrus (B = 2186.39, 95% CI: [901.84, 3470.95], p = 0.024). There were no significant differences in global efficiency between groups (B = 3.31, 95% CI: [-10.78, 17.40], p = 0.64). Results of all analyses with graph theory variables are reported in the Supplement (Tables S4 and S5).

Unharmonised data analyses

Analyses with unharmonised data yielded outcomes that were consistent (in direction, and generally size and significance) with outcomes of harmonised data analyses. Full results are reported in the Supplement (Tables S7-S9).

Association of structural connectome metrics and AN severity

Results of the exploratory analyses are presented in Table 3. Amongst AN, the scaled BMI variable was positively associated with connectivity within the subcortical component (B = 0.22, 95% CI: [0.06, 0.38], p = 0.007). Illness duration was not significantly associated with any of the structural connectivity measures.

Table 2: Outcomes of linear regression analyses exploring associations of illness severity markers with identified structural connectome differences amongst individuals with AN

Predictor variable[a]	**Association with BMI(kg/m^2)[bd]**		**Association with Illness Duration[c]**	
Structural connectivity metric	B [95% CI]	P-value	B [95% CI]	P-value
Subcortical component connectivity	0·2 [0·04,0·36]	0·02	-0·02 [-0·14,0·1]	0·78
Cortical component connectivity	-0·14 [-0·3,0·02]	0·10	0·01 [-0·11,0·13]	0·88
Strength of left parahippocampal gyrus	0·1 [-0·07,0·26]	0·25	-0·02 [-0·13,0·1]	0·77
Strength of left cerebellem	0·04 [-0·13,0·2]	0·67	0 [-0·11,0·12]	0·98
Strength of left hippocampus	0·1 [-0·06,0·26]	0·23	-0·05 [-0·17,0·07]	0·40
Strength of right lateral occipital gyrus	0·03 [-0·14,0·2]	0·76	0·08 [-0·04,0·2]	0·21
Strength of right cerebellem	0·06 [-0·11,0·22]	0·50	-0·01 [-0·13,0·11]	0·83

BMI: body mass index. [a]Predictors and outcome variables were mean centred and scaled. [b]Models adjusted for age, motion and study. [c]Models adjusted for age, motion, study, and the scaled BMI variable.[d]The BMI variable combined scaled BMI scores calculated in adults of the sample (aged over 19 years) with scaled BMI percentile scores calculated in adolescents (aged 19 years and below).

Subtype differences

Individuals with AN binge-purge subtype had greater strength of the right cerebellum relative to individuals with AN restricting subtype. There were no other significant differences between AN subtypes in terms of structural connectivity metrics (Supplementary material, Table S10).

Discussion

The current study harmonised data across multiple studies to reconstruct anatomical connections of the brain using probabilistic tractography, in a large sample of individuals with AN and HC. Analyses yielded a comprehensive description of the structural connectome in AN, including subnetwork and regional connectivity. The network-based statistic indicated that, relative to HC, individuals with AN had reduced connectivity within a component comprising connections between structures located subcortically in the brain. In contrast, patients displayed enhanced

connectivity in a cluster of tracts connecting regions of the frontal cortex, as compared to HC. The node-based analysis findings were consistent with network-based statistic outcomes: individuals with AN had reduced whole-brain connectivity of regions within the subcortical component. Amongst individuals with AN, lower BMI was associated with reduced connectivity within the subcortical component, highlighting an association between structural brain connectivity and illness severity in AN.

While this study did not measure behaviour directly, the finding of heightened connectivity in the frontal lobe along with weaker connectivity between subcortical regions is consistent with several proposed neurobiological models of AN. Heightened cortical connectivity, particularly between inferior frontal, lateral orbitofrontal, and anterior cingulate regions implicated in cognitive control, may relate to the highly inflexible behaviour observed in patients (50). Weakening within subcortical circuits may relate to decreased appetitive drive (51). These alterations may together support the persistent restriction of food intake that is the central behavioural characteristic of AN (52). The structural differences present amongst individuals with AN may underpin the alterations reported in functional MRI studies. In particular, reduced connectivity between subcortical regions (e.g., amygdala, thalamus), and altered connectivity within networks comprising frontal and cingulate regions, has been reported amongst individuals with AN, relative to HC, at rest (53). Altered activation within frontal brain regions during cognitive tasks is also reported amongst individuals with AN, as compared to HC (54).

Our findings are consistent with some earlier dMRI studies probing white matter properties that have reported individuals with AN, as compared with HC, to have greater integrity within frontal

portions of the inferior fronto-occipital fasciculus (55, 56), and reduced integrity of white matter in the fornix (13). The inferior fronto-occipital fasciculus traverses the inferior frontal and ventromedial regions in which elevated connectivity was seen amongst individuals with AN in the current study. The fornix is the major output tract of the hippocampus and encompasses white matter within the subcortical component in which we identified reduced connectivity amongst individuals with AN (e.g., connections between hippocampus, thalamus, parahippocampal cortex and entorhinal cortex).

The current findings do not precisely replicate prior investigations of region-to-region white matter connectivity in AN. Several investigations identified stronger connectivity in intra-hemispheric frontostriatal tracts amongst individuals with AN, both between the nucleus accumbens and OFC (14, 57), and between the putamen and motor areas (58). Studies observing elevated frontostriatal connectivity in AN patients adopted a region of interest approach, whereby the unit of analysis was single connections between brain regions. The current study tested differences at the level of subnetworks (or constellations of connected white matter connections), meaning inferences about differences within certain tracts cannot be made. Different analytical approaches could explain inconsistencies in findings relating to connectivity alterations within frontostriatal circuits amongst individuals with AN.

One large-scale tractography study of AN applied a brain-wide approach and probed network-level characteristics. This study reported greater integrity of white matter in occipital-parietal regions amongst individuals with AN, though no between-group differences in streamline counts (17). The earlier study used a tract reconstruction method based on the presence of a single fibre

direction per voxel, which may have contributed to the discrepancy between outcomes of the earlier study and outcomes of the current study. Single-fibre methods produce different (and less biologically accurate) reconstructions of white matter pathways relative to the multi-fibre probabilistic approach implemented herein (18-20). Replication attempts that implement similar tract reconstruction and analytical methods to those of the current study are necessary to evaluate the reliability and validity of inferences concerning brain organisation in AN that arise from this investigation.

Several limitations of this study should be considered. First, the data are cross-sectional, meaning causes and consequences of starvation cannot be parsed. Longitudinal studies may provide insight into whether the structural connectivity associated with AN in this study predicts illness onset/maintenance, or normalises with weight gain. Second, dMRI data were not optimal for constrained spherical deconvolution-based tractography. Ideally, dMRI scans would have been acquired with higher b-values (e.g., 3000), for more precise estimation of fibre orientation distributions within a given voxel. However even at low b-values, constrained spherical deconvolution-based tractography outperforms methods assuming a single-fibre orientation within each voxel, in terms of producing an anatomically accurate reconstruction of white matter pathways (59). Third, data harmonisation does not completely remove batch effects, and collecting all dMRI data in one study would have been ideal.

In summary, this large-scale investigation of whole-brain structural connectivity in patients with AN implemented advances in diffusion tractography and graph theory to yield information about the neural architecture associated with AN. Individuals with AN had reduced connectivity of and

between subcortical regions, and elevated connectivity within tracts connecting frontal regions. The identified connectivity profile hints at weaker processing within motivational networks, and greater processing within networks supporting cognitive control, the combination of which may drive restrictive eating behaviour. Future investigations using improved dMRI data acquisition parameters should seek to confirm our findings, and, using longitudinal designs, elucidate the nature of association between structural connectivity features and AN pathology.

Author Statements

Funding and disclosures

Funding

The study was supported by funding from the following sources: Global Foundation for Eating Disorders; Klarman Family Foundation; Translating Duke Health Initiative; NIMH (MH099388, MH076195, MH110445, MH105452, MH079397, MH113737).

Disclosures

Dr. Steinglass reports receiving royalties from UpTo Date. Dr. Posner has received support from Takeda (formerly Shire), Aevi Genomics, and Innovation Sciences. Dr Lloyd, Dr Foerde, Ms Aw, Mr Semanek, and Dr Muratore have no conflicts of interest to report.

Author contributions

ECL developed the analysis plan, and completed MRI preprocessing, diffusion tractography, data aggregation/harmonisation and data analysis, and drafted the manuscript. KEF refined the analysis plan and manuscript drafts. NA developed the diffusion imaging preprocessing and tractography pipelines for the current study and assisted with diffusion MRI preprocessing and diffusion tractography. DS assisted with preprocessing of the structural MRI data. AFM contributed to data aggregation and harmonisation. JES and JP designed the study and refined the analysis plan and manuscript drafts. All authors approved the final submission.

References

1. American Psychiatric Association. Diagnostic and statistical manual of mental disorders (DSM-5®): American Psychiatric Pub; 2013.
2. Arcelus J, Mitchell AJ, Wales J, Nielsen S. Mortality rates in patients with anorexia nervosa and other eating disorders. A meta-analysis of 36 studies. Arch Gen Psychiatry. 2011;68(7):724-31.
3. Mehler PS, Brown C. Anorexia nervosa - medical complications. J Eat Disord. 2015;3:11.
4. Ulfvebrand S, Birgegård A, Norring C, Högdahl L, von Hausswolff-Juhlin Y. Psychiatric comorbidity in women and men with eating disorders results from a large clinical database. Psychiatry Res. 2015;230(2):294-9.
5. Ágh T, Kovács G, Supina D, Pawaskar M, Herman BK, Vokó Z, et al. A systematic review of the health-related quality of life and economic burdens of anorexia nervosa, bulimia nervosa, and binge eating disorder. Eat Weight Disord. 2016;21(3):353-64.
6. Berends T, Boonstra N, van Elburg A. Relapse in anorexia nervosa: a systematic review and meta-analysis. Current opinion in psychiatry. 2018;31(6):445-55.
7. Lefco RW, Brissenden JA, Noyce AL, Tobyne SM, Somers DC. Gradients of functional organization in posterior parietal cortex revealed by visual attention, visual short-term memory, and intrinsic functional connectivity. Neuroimage. 2020;219:117029.
8. Friederici AD, Gierhan SME. The language network. Current Opinion in Neurobiology. 2013;23(2):250-4.
9. Chen T, Becker B, Camilleri J, Wang L, Yu S, Eickhoff SB, et al. A domain-general brain network underlying emotional and cognitive interference processing: evidence from coordinate-based and functional connectivity meta-analyses. Brain structure & function. 2018;223(8):3813-40.
10. Shen K, Hutchison RM, Bezgin G, Everling S, McIntosh AR. Network structure shapes spontaneous functional connectivity dynamics. Journal of Neuroscience. 2015;35(14):5579-88.
11. Horn A, Ostwald D, Reisert M, Blankenburg F. The structural–functional connectome and the default mode network of the human brain. Neuroimage. 2014;102:142-51.
12. Le Bihan D, Breton E, Lallemand D, Grenier P, Cabanis E, Laval-Jeantet M. MR imaging of intravoxel incoherent motions: application to diffusion and perfusion in neurologic disorders. Radiology. 1986;161(2):401-7.
13. Gaudio S, Carducci F, Piervincenzi C, Olivo G, Schiöth HB. Altered thalamo–cortical and occipital–parietal–temporal–frontal white matter connections in patients with anorexia and bulimia nervosa: a systematic review of diffusion tensor imaging studies. Journal of psychiatry & neuroscience: JPN. 2019;44(5):324.
14. Cha J, Ide JS, Bowman FD, Simpson HB, Posner J, Steinglass JE. Abnormal reward circuitry in anorexia nervosa: A longitudinal, multimodal MRI study. Human brain mapping. 2016;37(11):3835-46.
15. Sporns O, Tononi G, Kötter R. The human connectome: a structural description of the human brain. PLoS computational biology. 2005;1(4):e42.
16. Collantoni E, Alberti F, Meregalli V, Meneguzzo P, Tenconi E, Favaro A. Brain networks in eating disorders: a systematic review of graph theory studies. Eating and Weight Disorders-Studies on Anorexia, Bulimia and Obesity. 2021:1-15.

17. Geisler D, King JA, Bahnsen K, Bernardoni F, Doose A, Müller DK, et al. Altered White Matter Connectivity in Young Acutely Underweight Patients With Anorexia Nervosa. Journal of the American Academy of Child & Adolescent Psychiatry. 2021.
18. Tournier JD, Calamante F, Connelly A. MRtrix: Diffusion tractography in crossing fiber regions. International Journal of Imaging Systems and Technology. 2012;22(1):53-66.
19. Farquharson S, Tournier J-D, Calamante F, Fabinyi G, Schneider-Kolsky M, Jackson GD, et al. White matter fiber tractography: why we need to move beyond DTI. Journal of neurosurgery. 2013;118(6):1367-77.
20. Tournier J-D, Mori S, Leemans A. Diffusion tensor imaging and beyond. Magnetic resonance in medicine. 2011;65(6):1532-56.
21. Foerde K, Steinglass JE, Shohamy D, Walsh BT. Neural mechanisms supporting maladaptive food choices in anorexia nervosa. Nat Neurosci. 2015;18(11):1571-3.
22. Foerde K, Schebendach JE, Davis L, Daw N, Walsh BT, Shohamy D, et al. Restrictive eating across a spectrum from healthy to unhealthy: behavioral and neural mechanisms. Psychological Medicine. 2020:1-10.
23. Uniacke B, Wang Y, Biezonski D, Sussman T, Lee S, Posner J, et al. Resting-state connectivity within and across neural circuits in anorexia nervosa. Brain and behavior. 2019;9(1):e01205.
24. Lloyd EC, Foerde, K., Posner, J.P., & Steinglass, J., editor Longitudinal assessment of neural circuits in adolescents with anorexia nervosa: preliminary behavioral findings. Eating Disorders Research Society annual meeting; 2020.
25. Fairburn CG, Wilson GT, Schleimer K. Binge eating: Nature, assessment, and treatment: Guilford Press New York; 1993.
26. Sysko R, Glasofer DR, Hildebrandt T, Klimek P, Mitchell JE, Berg KC, et al. The eating disorder assessment for DSM-5 (EDA-5): Development and validation of a structured interview for feeding and eating disorders. The International journal of eating disorders. 2015;48(5):452-63.
27. Team RC. R: A Language and Environment for Statistical Computing. R Foundation for Statistical Computing; 2017.
28. First MB. Structured clinical interview for the DSM (SCID). The encyclopedia of clinical psychology. 2014:1-6.
29. Kaufman J, Birmaher B, Brent D, Rao U, Flynn C, Moreci P, et al. Schedule for affective disorders and schizophrenia for school-age children-present and lifetime version (K-SADS-PL): initial reliability and validity data. Journal of the American Academy of Child & Adolescent Psychiatry. 1997;36(7):980-8.
30. Fischl B. FreeSurfer. Neuroimage. 2012;62(2):774-81.
31. Fischl B, Salat DH, Busa E, Albert M, Dieterich M, Haselgrove C, et al. Whole brain segmentation: automated labeling of neuroanatomical structures in the human brain. Neuron. 2002;33(3):341-55.
32. Desikan RS, Ségonne F, Fischl B, Quinn BT, Dickerson BC, Blacker D, et al. An automated labeling system for subdividing the human cerebral cortex on MRI scans into gyral based regions of interest. Neuroimage. 2006;31(3):968-80.
33. Tournier JD, Smith R, Raffelt D, Tabbara R, Dhollander T, Pietsch M, et al. MRtrix3: A fast, flexible and open software framework for medical image processing and visualisation. NeuroImage. 2019;202:116137.

34. Andersson JLR, Sotiropoulos SN. An integrated approach to correction for off-resonance effects and subject movement in diffusion MR imaging. NeuroImage. 2016;125:1063-78.
35. Tustison NJ, Avants BB, Cook PA, Zheng Y, Egan A, Yushkevich PA, et al. N4ITK: improved N3 bias correction. IEEE transactions on medical imaging. 2010;29(6):1310-20.
36. Smith SM, Jenkinson M, Woolrich MW, Beckmann CF, Behrens TEJ, Johansen-Berg H, et al. Advances in functional and structural MR image analysis and implementation as FSL. NeuroImage. 2004;23:S208-S19.
37. Jenkinson M, Smith S. A global optimisation method for robust affine registration of brain images. Medical Image Analysis. 2001;5(2):143-56.
38. Jenkinson M, Bannister P, Brady M, Smith S. Improved Optimization for the Robust and Accurate Linear Registration and Motion Correction of Brain Images. NeuroImage. 2002;17(2):825-41.
39. Dhollander T, Mito R, Raffelt DC, A. Improved white matter response function estimation for 3-tissue constrained spherical deconvolution. . Proc Intl Soc Mag Reson Med. 2019:555.
40. Tournier JD, Calamante F, Connelly A. Robust determination of the fibre orientation distribution in diffusion MRI: Non-negativity constrained super-resolved spherical deconvolution. NeuroImage. 2007;35(4):1459-72.
41. Tournier JD, Calamante F, Connelly A, editors. Improved probabilistic streamlines tractography by 2nd order integration over fibre orientation distributions. Proceedings of the international society for magnetic resonance in medicine; 2010: John Wiley & Sons, Inc. New Jersey, USA.
42. Smith RE, Tournier J-D, Calamante F, Connelly A. Anatomically-constrained tractography: Improved diffusion MRI streamlines tractography through effective use of anatomical information. NeuroImage. 2012;62(3):1924-38.
43. Fortin J-P, Parker D, Tunç B, Watanabe T, Elliott MA, Ruparel K, et al. Harmonization of multi-site diffusion tensor imaging data. NeuroImage. 2017;161:149-70.
44. Fortin J-P, Cullen N, Sheline YI, Taylor WD, Aselcioglu I, Cook PA, et al. Harmonization of cortical thickness measurements across scanners and sites. Neuroimage. 2018;167:104-20.
45. Civier O, Smith RE, Yeh C-H, Connelly A, Calamante F. Is removal of weak connections necessary for graph-theoretical analysis of dense weighted structural connectomes from diffusion MRI? NeuroImage. 2019;194:68-81.
46. Zalesky A, Fornito A, Bullmore ET. Network-based statistic: identifying differences in brain networks. Neuroimage. 2010;53(4):1197-207.
47. MATLAB. MATLAB. version 9.6.0.1072779 (2019a) ed. Natick, Massachusetts2019.
48. Rubinov M, Sporns O. Complex network measures of brain connectivity: Uses and interpretations. NeuroImage. 2010;52(3):1059-69.
49. Frossard Renaud O, @font-face, {font-family:&amp, quot, Math&amp C, quot, et al. Permuco: Permutation Tests for Regression, (Repeated Measures) ANOVA/ANCOVA and Comparison of Signals. R package version 1.1.0. ed2019.
50. Walsh BT. The enigmatic persistence of anorexia nervosa. Am J Psychiatry. 2013;170(5):477-84.
51. Kaye, Fudge, Paulus. New insights into symptoms and neurocircuit function of anorexia nervosa. Nat Rev Neurosci. 2009;10(8):573-84.

52. Walsh BT. The importance of eating behavior in eating disorders. Physiol Behav. 2011;104(4):525-9.
53. Gaudio S, Wiemerslage L, Brooks SJ, Schiöth HB. A systematic review of resting-state functional-MRI studies in anorexia nervosa: evidence for functional connectivity impairment in cognitive control and visuospatial and body-signal integration. Neuroscience & Biobehavioral Reviews. 2016;71:578-89.
54. Wonderlich JA, Bershad M, Steinglass JE. Exploring Neural Mechanisms Related to Cognitive Control, Reward, and Affect in Eating Disorders: A Narrative Review of FMRI Studies. Neuropsychiatric disease and treatment. 2021;17:2053-62.
55. Vogel K, Timmers I, Kumar V, Nickl-Jockschat T, Bastiani M, Roebroek A, et al. White matter microstructural changes in adolescent anorexia nervosa including an exploratory longitudinal study. NeuroImage Clinical. 2016;11:614-21.
56. Frank GKW, Shott ME, Hagman JO, Yang TT. Localized brain volume and white matter integrity alterations in adolescent anorexia nervosa. Journal of the American Academy of Child and Adolescent Psychiatry. 2013;52(10):1066-75.e5.
57. Frank G, Shott M, Riederer J, Pryor T. Altered structural and effective connectivity in anorexia and bulimia nervosa in circuits that regulate energy and reward homeostasis. Translational psychiatry. 2016;6(11):e932-e.
58. Tadayonnejad R, Pizzagalli F, Murray SB, Pauli WM, Conde G, Bari AA, et al. White matter tracts characteristics in habitual decision-making circuit underlie ritual behaviors in anorexia nervosa. Scientific Reports. 2021;11(1):15980.
59. Calamuneri, A., Arrigo, A., Mormina, E., Milardi, D., Cacciola, A., Chillemi, G., Marino, S., Gaeta, M., & Quartarone, A. (2018). White Matter Tissue Quantification at Low *b*-Values Within Constrained Spherical Deconvolution Framework. *Frontiers in neurology*, *9*, 716. https://doi.org/10.3389/fneur.2018.00716

Figure legends

Figure 1: Neuroimaging and analysis methods of the current study
Caption: For each participant, a diffusion MRI and structural MRI scan were acquired (panel A). White matter tracts in the brain were reconstructed using a probabilistic tracking algorithm applied to diffusion MRI data, and the structural brain image was parcellated into 84 regions (panel B). Combining the tractography output with the brain parcellation allowed the creation of a structural connectome for each participant, which described the number of streamlines between each pair of regions (panel C). This information was represented in a weighted adjacency matrix, which was used to calculate node metrics (panel D). Anorexia nervosa and healthy control groups were compared on the strength of structural connections and node metrics, across the whole brain (panel E).

Figure 2: Results of the network-based statistic analysis
Caption: Panel A shows the component comprising tracts that had higher streamline counts in healthy control participants compared to AN patients. Panel B shows the component comprising tracts that had higher streamline counts in AN patients compared to healthy control participants. AN: anorexia nervosa, HC: healthy controls, lLOF: left lateral orbitofrontal gyrus, lpOPER: left pars opercularis, lpORB: left pars orbitalis, lpreC: left precentral gyrus, lSTG: left superior temporal gyrus' rFP: right frontal pole, rPUT: right putamen, rrACC: right rostral anterior cingulate gyrus, lCer: left Cerebellum, lFP: left frontal pole, lLOF: left lateral orbitofrontal, lPARH: left parahippocampal gyrus, lTHAL: left thalamus, rHIPP: right hippocampus, rPARH: right parahippocampal gyrus, rTHAL: right thalamus.